Accepted Manuscript

A parameter for quantitative analysis of plasticity induced crack closure

F.V. Antunes, L. Correia, A.L. Ramalho

PII: S0142-1123(13)00247-8
DOI: http://dx.doi.org/10.1016/j.ijfatigue.2013.08.026
Reference: JIJF 3203

To appear in: *International Journal of Fatigue*

Received Date: 11 June 2013
Revised Date: 28 August 2013
Accepted Date: 30 August 2013

Please cite this article as: Antunes, F.V., Correia, L., Ramalho, A.L., A parameter for quantitative analysis of plasticity induced crack closure, *International Journal of Fatigue* (2013), doi: http://dx.doi.org/10.1016/j.ijfatigue.2013.08.026

This is a PDF file of an unedited manuscript that has been accepted for publication. As a service to our customers we are providing this early version of the manuscript. The manuscript will undergo copyediting, typesetting, and review of the resulting proof before it is published in its final form. Please note that during the production process errors may be discovered which could affect the content, and all legal disclaimers that apply to the journal pertain.

ACCEPTED MANUSCRIPT

A parameter for quantitative analysis of plasticity induced crack closure

FV Antunes[1,*], L Correia[2], AL Ramalho[2]
[1)] CEMUC, Department of Mechanical Engineering, University of Coimbra
Rua Luís Reis Santos, Pinhal de Marrocos, 3030-788 Coimbra, Portugal
E-mail: fernando.ventura@dem.uc.pt
[2)] CEMUC, Escola Superior de Tecnologia do Instituto Politécnico de Castelo Branco
Av. do Empresário, 6000 - 767 Castelo Branco
E-mail: lcorreia@ipcb.pt; aramalho@ipcb.pt

Abstract

Numerical models have been successfully developed to predict plasticity induced crack closure (PICC). However, despite the large research effort a full understanding of the links between physical parameters, residual plastic wake and PICC has not been achieved yet. The plastic extension of material behind crack tip, Δy_p, obtained by the integration of vertical plastic deformation perpendicularly to crack flank, is proposed here to quantify the residual plastic field. The values of Δy_p and PICC were obtained numerically in a M(T) specimen using the finite element method. An excellent correlation was found between PICC and Δy_p which indicates that this parameter controls the phenomenon, and can be used to quantify the effect of physical parameters. An empirical model was developed to predict PICC assuming that the residual plastic field is a set of vertical plastic wedges, that the linear superposition principle applies and that the influence of a particular wedge exponentially decreases with distance to crack tip. The model was applied successfully to predict PICC for different residual plastic fields which provided an additional validation of Δy_p as the parameter controlling PICC.

Keywords

Plasticity induced crack closure (PICC); finite element method; plastic wedges; residual plastic field

1. Introduction

In flawed or notched components submitted to cyclic loading crack propagation usually occupies a significant part of the fatigue life. The defects may be caused by technological processes like welding, casting or machining. Crack closure is an extrinsic phenomenon affecting fatigue crack propagation and must be included in fatigue design. Crack closure is the contact of the fracture surfaces during a portion of the load cycle, and is usually associated with plastic deformation, oxide particles or roughness at the crack flanks [1-3]. This contact is

* Corresponding author: e-mail: fernando.ventura@dem.uc.pt; Fax: 00351 239 790701

ACCEPTED MANUSCRIPT

expected to affect the local stress and strain fields near the crack tip, and therefore the intrinsic micromechanisms responsible for fatigue crack propagation. In fact, current application of fracture mechanics concepts to fatigue crack advance characterization are generally based on the premise that the compression part of the fatigue cycles does not contribute to fatigue damage. Crack closure seems to be able to explain the influence of mean stress in both regimes I and II of crack propagation [4,5], the transient crack growth behavior following overloads [6], the growth rate of short cracks [7] and the effect of thickness on fatigue crack propagation [8,9]. The shielding effect produced by crack closure can also explain the increase of crack propagation life with increasing stress concentration in circumferentially notched bars fatigued under cyclic torsion [10-12]. According to Elber's understanding of crack closure [4,13], as the crack propagates due to cyclic loading a residual plastic wake is formed. The plastically deformed material acts as a wedge behind the crack tip promoting the contact of fracture surfaces during the elastic recovery of the surrounding material. Numerical models have been successfully developed to predict plasticity induced crack closure (PICC) and to understand the basic mechanisms behind it [14]. These studies focused on the optimization of the large number of numerical parameters [15-17] and on the influence of physical parameters such as crack shape, stress state or variable amplitude loading [18,19] on PICC. However, despite the significant research effort, the full understanding of the links between physical parameters, the residual strain field and PICC has not been achieved yet.

PICC is intimately linked to the crack tip plastic deformation. The forward plastic zone is constituted by the material near the crack tip undergoing plastic deformation during loading, while the reversed plastic zone is formed by the material undergoing compressive yielding during unloading. The increase of monotonic plastic deformation increases the PICC level, and the increase of reversed plastic deformation has the opposite effect. The monotonic plastic deformation increases with maximum load and crack length (i.e., with K_{max}), while the

ACCEPTED MANUSCRIPT

reversed deformation depends on ΔK and material behavior. In materials with significant Bauschinger effect, important deformation occurs during unloading, reducing closure level and compressive residual stresses. Accordingly, the use of pure kinematic hardening models was found to produce the largest reversed plastic zones, while the pure isotropic models were found to produce the smallest zones [20]. The strain ratcheting phenomenon also determines the residual plastic field [20, 21].

The effect of physical parameters on residual plastic field has been studied using different approaches. The analysis of stress-strain curves at specific Gauss points (GP) has been widely used [22-24], since it provides interesting information concerning plastic deformation generation. As the crack tip approaches the Gauss point, plastic deformation increases progressively. A peak of deformation exists when the GP is at the closest position ahead of crack tip and the phenomenon stops when the crack tip moves ahead of the GP. However, these curves only permit a qualitative analysis of the effect of parameters. Therefore, alternative approaches were considered in literature to quantify residual plastic field, like the analysis of crack profile [24]. The difference of opening between the stationary and the fatigue cracks reflects the amount of residual plastic deformation left by the cyclic loading [25-27]. Singh *et al.* [28] used it to study the effect of repeated overloads, and Roychowdhury *et al.* [29] studied the effect of T-stress. Vor *et al.* [30] considered $\Delta\varepsilon_{22}$ and ΔCTOD, the strain range at the crack tip (2 is the loading direction) and the crack tip opening displacement range, respectively. Zhao *et al.* [24] and Roychowdhury *et al.* [27] studied the plastic strains (ε_{px}, ε_{py}, ε_{pz}) along the crack path, while Matos *et al.* [31] analyzed the contact stresses. A parameter is however missing, which is representative of all residual plastic field and can be used to establish quantitative links between physical parameters, residual deformation and PICC level.

A parameter is therefore proposed here, which is the plastic extension of material behind crack tip, Δy_p, obtained by the integration of vertical plastic deformation perpendicularly to

ACCEPTED MANUSCRIPT

crack flank. This parameter is expected to control the PICC level because of the evident physical sense. The values of Δy_p and PICC are obtained numerically using the finite element method. An empirical model is developed in order to validate the concept proposed, assuming that the residual plastic field is a set of vertical plastic wedges, that the linear superposition principle applies and that the influence of a particular wedge decreases exponentially with distance to crack tip.

2. Numerical model

Figure 1 illustrates the geometry of the Middle-cracked Tension (M(T)) specimen studied here, which is in agreement with ASTM E647 standard. An initial crack length a_0=5 mm was modelled, therefore a_0/W=0.083, being *W* the specimen's width. Due to the symmetry of the sample in terms of geometry, material properties and loading, only 1/8 of the M(T) specimen was simulated by using appropriate boundary conditions. The thickness considered in the numerical model was t/2=0.1 mm which corresponds to a specimen thickness of 0.2 mm. The opposite crack surface was simulated by assuming frictionless contact conditions over a rigid symmetry plane placed behind the growing crack front. As illustrated in figure 2, different loading conditions were considered in the investigation, namely, constant amplitude loading (Fig. 2a), single overloads (Fig. 2b), and loading blocks (Fig. 2c). A load cycle applied at the beginning of crack propagation and followed by relatively low amplitude levels was also considered (Fig. 2d). The loads considered in the constant amplitude tests are presented in Table 1. The overload ratio was defined as:

$$\mathrm{OLR} = \frac{\mathrm{F_{ol}} - \mathrm{F_{min}}}{\mathrm{F_{max}} - \mathrm{F_{min}}} \tag{1}$$

where F_{min}, F_{max} and F_{ol}, are the minimum, maximum and overload forces, respectively. The material parameters used in the numerical simulations corresponded to the 6016-T4 aluminium alloy (92 HV0.5). Since the PICC phenomenon is a consequence of crack tip plastic

ACCEPTED MANUSCRIPT

deformation, the plastic behaviour must be carefully modelled. In the present work, an anisotropic yield criterion [32] was considered, which is expressed by the quadratic function:

$$F\left(\sigma_{yy}-\sigma_{zz}\right)^2+G\left(\sigma_{zz}-\sigma_{xx}\right)^2+H\left(\sigma_{xx}-\sigma_{yy}\right)^2+2L\tau_{yz}^{\ 2}+2M\tau_{zx}^{\ 2}+2N\tau_{xy}^{\ 2}=1 \quad (2)$$

where σ_{xx}, σ_{yy}, σ_{zz}, τ_{xy}, τ_{xz} and τ_{yz} are the components of the effective stress tensor defined in the orthotropic frame and *F*, *G*, *H*, *L*, *M* and *N* are coefficients that characterize the anisotropy of the material. In order to characterize the hardening behavior of the aluminium alloy, three types of mechanical tests were performed: uniaxial tensile tests and monotonic and Bauschinger shear tests. From the experimental data and curve fitting results [33], for different constitutive models, it was determined that the mechanical behavior of this alloy is accurately modelled using a Voce type equation:

$$Y=Y_0+R_{sat}(1-e^{-n_v\bar{\varepsilon}^p}), \quad (3)$$

to describe the isotropic component of hardening, combined with the saturation law:

$$\dot{X}=C_x\left[X_{sat}\frac{\left(\sigma'-X\right)}{\bar{\sigma}}-X\right]\dot{\bar{\varepsilon}}^p, \quad (4)$$

to describe the kinematic component of hardening. In these equations *Y* is the equivalent flow stress, $\bar{\varepsilon}^p$ is the equivalent plastic strain, Y_0 is the initial yield stress, R_{sat} is the saturation stress, n_v, C_x and X_{sat} are material constants, $\boldsymbol{\sigma}'$ is the deviatoric stress tensor, *X* is the back stress tensor, $\dot{\bar{\varepsilon}}^p$ the equivalent plastic strain rate and $\bar{\sigma}$ the equivalent stress. The material constants used in the numerical simulations were: Y_0=124 MPa, R_{sat}=291 MPa, n_v= 9.5, C_x= 146.5 and X_{sat} = 34.90 MPa, *F*=0.5998; *G*=0.5862; *H*=0.4138; *L*=1.2654; *M*=1.2654; *N*=1.2654.

Figure 3 presents the finite element mesh used in the investigation, which was refined at the crack front, to enable the numerical simulation of the severe plastic deformation gradients, and enlarged at remote positions, to reduce the numerical effort. It is a 3D model with only one

ACCEPTED MANUSCRIPT

layer of finite elements in the thickness direction. Notice that the software, which is highly competent in plastic deformation modelling, is limited to 3D models. The sizes considered for the square elements placed around the crack front were L_1=8 μm (mesh M8), L_1=16 μm (mesh M16) or L_1=32 μm (mesh M32), and the total number of linear isoparametric elements and nodes were (6169, 12632), (2587, 5382) and (1275, 2712), respectively. The coordinate system considered to define the numerical model is indicated in figure 3.

Crack propagation was simulated by successive debonding of nodes at minimum load. Each crack increment (Δa_i) corresponded to one finite element and two load cycles were applied between crack increments. In each cycle, the crack propagated uniformly over the thickness by releasing both crack front nodes. Crack extensions of 0.96 mm were simulated, which correspond to 60 crack propagations for mesh M16. The opening load, F_{op}, was determined by evaluating the contact status of the first node behind current crack tip with the symmetry plane. Considering the discrete character of the finite element simulations, the exact opening load was obtained from the linear extrapolation of the loads corresponding to the two increments following opening. The PICC level was measured at the free surface of the specimen, therefore corresponds to a plane stress state.

The numerical simulations were performed with a three-dimensional elastic-plastic finite element program (DD3IMP) that follows a fully implicit time integration scheme [34, 35]. The mechanical model and the numerical methods used in the finite element code, specially developed for the numerical simulation of metal forming processes, takes into account the large elastic-plastic strains and rotations occurring during large deformation processes. To avoid the locking effect, a selective reduced integration scheme was used [36, 37]. The optimum values for the numerical parameters of the DD3IMP implicit algorithm had been already established in previous works, concerning the numerical simulation of sheet metal forming processes [38] and PICC [39].

ACCEPTED MANUSCRIPT

3. Numerical results

3.1. Generation of the residual plastic wake

Figure 4a presents the stress-strain curve σ_{yy}-ε_{yy} registered at a Gauss point (GP) during crack propagation. The stresses were normalized by the yield stress of the aluminium alloy (124.2 MPa). Figure 4b shows the Gauss point and the successive positions of crack tip. At the beginning of crack propagation, the Gauss point is 28.3 finite elements ahead of crack tip, which corresponds to 451 μm since the local mesh is composed of square elements with 16×16 μm^2. Although this initial distance, the GP suffers some plastic deformation, which indicates that it is within the first forward plastic zone. A compressive stress state is observed at minimum load but no reversed plasticity occurs. As the crack propagates the distance of the GP relatively to the crack tip reduces, and the stress level increases producing more plastic deformation. The compressive stress at minimum load also increases and starts producing reversed plastic deformation. The distance between the beginning of reversed plasticity and the GP defines the size of reversed plastic zone, which is about 6×16 μm=96 μm for the situation presented. In fact, the analysis of stress-strain curve is probably the best way to quantify this size. But the maximum plastic deformation happens when the GP is immediately ahead of crack tip, i.e., when the crack tip is at position 29 in figure 4b. The two load cycles applied between crack propagation are now clearly visible. The stress level reaches about 3 times material's yield stress, as a consequence of isotropic hardening. When the crack moves ahead of the GP (crack tip at position 30 in figure 4b), the stress level applied to the GP becomes relatively low and the plastic deformation ceases. The plastic deformation is now a residual deformation. The magnitude of residual plastic deformation in figure 4a is lower than 2%, therefore is relatively low. The finite element mesh, the maximum and minimum loads, the hardening properties, the stress state, etc, influence the stress-strain curve and therefore the residual plastic deformation. The mesh refinement, for example, approaches the Gauss point to

ACCEPTED MANUSCRIPT

the crack face, therefore increases the stress and strain levels. The effect of different physical and numerical parameters on stress-strain curves has been widely studied on literature, as already mentioned [21-24].

Gauss points at greater distances from crack flank have a similar behaviour to that reported in figure 4, but lower stress and strain levels. Figure 5 plots the distribution of vertical strain, ε_{yy}, along a vertical line starting at the crack flank (y direction in figure 3), for different constant amplitude loading tests (K_{max}=4.6, 6.4 and 9.1 MPa.m$^{1/2}$) and two finite element meshes (M8 and M32). The strain values were measured at minimum load, being mainly composed of residual plastic deformation. However, the elements closer to the crack flank have compressive elastic deformation which explains the strain reduction observed for y<0.05 mm. The deformation level is more relevant near the symmetry plane decreasing substantially with *y* distance. The increase of the load level significantly increases the strain level, while the mesh refinement affects the plastic strain near the crack flank but has a limited influence far from this.

A new set of finite element models was developed to quantify the contributions of different finite element layers parallel to crack flank to PICC. In these models the yield stress of horizontal layers of finite elements, parallel to the crack flank, was increased to 350 MPa, layer by layer, from the crack flank up to the 10th layer. Figure 6a shows the PICC level versus the number of horizontal hard layers, for two constant amplitude loading tests (K_{max}=4.6 MPa.m$^{1/2}$, K_{min}=0; and K_{max}=6.4 MPa.m$^{1/2}$, K_{min}=0). Figure 6b shows the relative influence, in percentage, of each horizontal deformed layer on the global value of PICC. The first layer has always the most significant influence on PICC. The importance of horizontal layers decreases steadily with distance to crack flank which is according the results of figure 5. The increase of maximum load decreases the influence of the first layer on PICC (from 44 to 23.5%) and increases the importance of the most remote regions in the vertical direction (from 56 to

ACCEPTED MANUSCRIPT

76.5%). Careful is required to ensure that the plastic deformation wedge is included in the most refined region of the finite element mesh defined around the crack propagation region (see figure 3).

3.2. Magnitude of residual plastic wedge, Δy_p

The influence of physical and numerical parameters on residual plastic field has been widely studied, as already mentioned. However, the link between residual field and PICC is missing, mainly due to the lack of a single parameter able to encompass all plastic strain distribution. The parameter proposed here is the integration along *y* direction of the vertical plastic deformation, $\varepsilon_{p,yy}$:

$$\Delta y_p = \int_0^h \varepsilon_{p,yy}.dy \tag{5}$$

Δy_p has a physical meaning, which is the vertical elongation of all plastic wedge. In eq. (5), *h* represents the integration length which must be higher than the height of the plastic field. As already discussed, the segments closest to crack flank contribute more significantly to Δy_p. Values of Δy_p of 0.0005, 0.0011, 0.0013 and 0.0024 mm, were obtained for (M32, K_{max}=4.6 MPa.m$^{1/2}$), (M32, K_{max}=6.4 MPa.m$^{1/2}$), (M8, K_{max}=6.4 MPa.m$^{1/2}$) and (M32, K_{max}=6.4 MPa.m$^{1/2}$) curves in figure 5, respectively. These values were unexpectedly small, indicating that a small plastic extension is enough to produce PICC.

Figure 7 shows the relationship between plastic wedge magnitude, Δy_p, and the crack opening level quantified by the effective ratio, $\sigma_{open}/\sigma_{max}$. The results were obtained for a wide range of constant amplitude loading conditions. Sets with constant values of K_{max}, K_{min}, ΔK and R were considered. Results for a High Strength Steel (DP600) are also presented. A strong link is evident between PICC level and Δy_p which indicates that this parameter effectively characterizes the residual plastic field. According to the figure, the PICC level increases

ACCEPTED MANUSCRIPT

significantly for relatively low Δy_p values, and more moderately for relatively large values of Δy_p. It is interesting to notice that a similar behaviour was found for roughness induced crack closure [40,41].

3.3. Empirical model

An empirical model was developed considering that Δy_p is the parameter controlling the effect of residual plastic field on PICC and that:

- the linear superposition principle applies to the effect of individual plastic wedges behind crack tip. The residual plastic field is seen as a set of vertical plastic wedges;
- the influence of Δy_p decreases exponentially with distance to crack tip.

These assumptions are detailed studied next.

3.3.1. Linear superposition principle

In order to analyze the influence of vertical residual wedges on PICC, a parametric analysis was performed by manipulating the material properties of finite element model in order to create plastic wedges at specific locations along crack flank. More precisely, finite element models were generated in which soft material strips, having the material properties of the 6016-T4 aluminum alloy, were embedded in a surrounding hard material matrix simulated by increasing artificially the yield stress of the alloy (Y_0 = 9524 MPa in Eq. (3)). The yield stress of the hard matrix was defined in order to insure that plastic deformation during cyclic loading was restricted to the soft material columns distributed along the crack flank. Figure 8 illustrates the finite element model with the vertical plastic wedges embedded in the hard matrix. Each plastic wedge is constituted by only one column of finite elements. The different soft plastic wedges were identified according to their location relatively to the initial crack tip position (20^{th}, 30^{th} and 40^{th} finite element columns, as indicated in figure 8). The crack was propagated and the PICC level was measured when the crack tip was at the 40^{th} position. It was

ACCEPTED MANUSCRIPT

found that the plastic deformation of the 20th column (figure 8a) affects the PICC measured at the 40th column; and that the effect of the plastic deformation of the 30th column (figure 9b) on the PICC level measured at the 40th column is higher than for the 20th column. Moreover, the PICC level from the 20th column (figure 8a) plus the PICC level from the 30th column (figure 8b) is nearly equal to the effect of both columns simultaneously (figure 8c), with a difference of only about 0.5%. This study was repeated for different number and locations of the individual plastic wedges along the hardened crack flank, always with the same result. Therefore, it was concluded that the linear superposition effect applies to the effect of individual plastic wedges on PICC level. Notice that behind the current crack tip the residual plastic wedges behave elastically, therefore the applicability of the superposition principle is not surprising.

3.3.2. PICC versus distance to crack tip

The approach illustrated in figure 8 was also used to study the effect of distance to crack tip. Different finite element models were defined with only two element columns of soft material (as figures 8a and 8b illustrate). One of the columns was fixed at the 40th position relatively to the initial crack position. The second element column was placed at different positions relatively to the 40th column in each finite element model, with *d* being the distance between both columns. The yield stress of surrounding material was once again greatly increased to isolate the two plastic wedges, and the crack was propagated. Figure 9a shows the PICC level measured at the 40th element column versus *d* distance. The PICC level was quantified by the ratio between the opening and maximum loads, being the opening defined from the contact status of the first node behind crack tip. The column at a distance *d* was found to influence the PICC level measured at the 40th one. The PICC level reduces significantly with distance converging to zero for relatively large distances. This means that the influence of individual plastic wedges strongly decreases with distance to crack tip.

ACCEPTED MANUSCRIPT

A second example of the vanishing influence of plastic wedges is the evolution of PICC after overloads (load case schematized in figure 2b). As shown in the scheme inserted in figure 9b, *d* now corresponds to the distance between the overload peak and current crack tip position, and ΔPICC corresponds to the difference between the current PICC value and the PICC value for the constant amplitude loading. A homogeneous material model, corresponding to the behaviour of the 6016-T4 aluminium alloy was considered. The overload produces a PICC peak which asymptotically dissipates with crack propagation ahead of the region affected by the overload plastic deformation. Once again, there is a relatively fast dissipation of the effect with crack propagation ahead of the region affected by the initial plastic deformation. Notice that in this case several columns of finite elements are affected by the overload. A similar trend was obtained for a single load applied at the beginning of crack propagation (load case of figure 2d), which produces a single plastic deformation zone. Afterwards the crack was propagated at a relatively low load, and the opening level was measured at different positions. The results, which are presented, also showed a fast decrease of PICC level.

A fourth approach was considered to study the effect of distance to crack tip, consisting of constant amplitude loading tests in homogeneous material. It is well known that for constant amplitude load, the PICC level evolves with crack propagation, reaching stabilized values after a certain number of crack increments (figure 9c). The difference between the PICC levels corresponding to two consecutive crack tip positions, ΔPICC, indicates the influence of each crack increment on PICC. Notice that, as is schematically illustrated in figure 9d, crack propagation adds plastic wedges at the crack tip. Analyzing the situation from the point of view of the crack tip, it seems that for each crack propagation a plastic wedge is added at the most remote position along crack flank. In other words, if the co-ordinate system is placed always at the crack tip, it appears that a new wedge has appeared at a remote position from crack tip. The corresponding variation of the global PICC is the effect of this “new” plastic wedge at a

ACCEPTED MANUSCRIPT

distance *d*. This approach was found to be the best solution to isolate and quantify the effect of individual plastic wedges. Figure 9d shows the ΔPICC versus distance *d* for a constant amplitude load with K_{max}=6.5 MPa.m$^{1/2}$, K_{min}=0.1 N MPa.m$^{1/2}$ (σ_{max}/σ_{ys}=0.38, R=0.02). As can be seen, the effect of an individual plastic wedge on PICC strongly decreases with increasing distance to the crack tip (*d*), becoming close to zero when PICC stabilized values are reached. A comparative analysis of figures 9, corresponding to quite different physical situations, indicates that the influence of a plastic wedge rapidly decreases with distance to crack tip. Notice also that the effect of residual plastic wake disappears when the crack tip moves by less than one millimetre. In other words, the residual plastic wake affecting the PICC level is limited to less than one millimetre. Besides, the plastic layers up to 0.1 mm behind crack tip represent more than 50% of PICC level. In fact, a distance of 0.1 mm from crack tip was considered by Iyyer *et al.* [42] to analyse the contact status of crack flanks and therefore to define the crack opening level. The fast decrease of closure with distance to crack tip was also evident in studies of partial closure [43] and short cracks [44].

The rapid decrease of the influence of plastic wedges is explained in figure 10. Figure 10a shows schematically a vertical plastic wedge at a distance *d* from crack tip, at minimum load. The plastic wedge is compressed by the surrounding elastically deformed material. To open the crack a remote load is required, able to overcome the compressive residual force at the plastic wedge (Figure 10b). A parallel numerical study was developed to quantify the relation between the compressive force at the plastic wedge, F_p, the distance to crack tip, *d*, and the stress intensity factor required to open the crack. A punctual force was applied at the crack flank at a distance *d* from crack tip, and the stress intensity factor (K) was calculated from J-integral in a linear elastic analysis. The influence of punctual forces was found to strongly decrease as the distance *d* increases, approaching zero for large distances. A power type curve was fitted by regression to the numerical results:

ACCEPTED MANUSCRIPT

$$\frac{K_{open}}{F_p/(t.W)\sqrt{W}} = \frac{1.07}{(d/W)^{-0.465}} \quad (6)$$

being t=0.1×10^{-3}m and W=0.03 m the thickness and width of specimen's physical model, respectively. Additionally, the contact forces at minimum load decrease substantially from crack tip, as figure 11a shows. Christopher *et al.* [45] proposed a decay of contact stresses in the form of $d^{-1/2}$. These two effects, i.e., the decrease of contact forces and of their influence with distance to crack tip, explain the results of figure 9 concerning the variation of PICC. Solancki *et al.* [46] proposed a new approach to quantify the PICC level, based on the contact forces (instead of the contact status behind crack tip). Figure 11b shows the opening stress intensity factor versus distance to crack tip, obtained from contact forces at minimum load using equation 6. A strong decrease with distance to crack tip is evident reinforcing the results of figure 9. Also here it was observed that a significant portion of PICC level is related with the contact up to a distance of 0.1 mm behind crack tip. Looking once again to figure 10, it is evident that the compressive force depends on the plastic deformation level of the plastic wedge, i.e., depends on (y_o-y_i). Notice that Δy_p is the distance (y_o-y_i), having therefore a physical meaning as already stated.

3.3.3. PICC versus individual plastic wedges

The empirical model was developed based on the PICC numerical results. The basic idea was to establish a relationship between an individual plastic wedge, characterized by its position (d) and magnitude (Δy_p), and the PICC level. A major difficulty was the isolation of the effect of the individual plastic wedge, and different solutions were tried as illustrated in figure 9. The best solution found was that illustrated in figure 9d. In a constant amplitude crack growth test, the crack grows, i.e., the crack tip moves ahead. Adopting the crack tip as reference, it seems that an extra edge is added at the most remote position of residual plastic

ACCEPTED MANUSCRIPT

wake, which increases PICC level by Δ_{PICC}. This Δ_{PICC} value is therefore the influence of a plastic wedge of magnitude Δy_p at a distance d (i.e., $PICC_i=\Delta_{PICC}$). A link may be established between the position of this plastic wedge, its magnitude and the PICC variation. Figure 12a shows the PICC increase versus distance to crack tip, for different values of remote loading. The increase of d strongly decreases PICC, as already discussed, while the increase of load level increases PICC. An excellent fitting was found with an exponential model:

$$PICC_i = \tilde{f}(d, \Delta y_p) = a \cdot d^b \quad (7)$$

being d the distance to crack tip, and a,b fitting constants dependent on Δy_p. Figures 12b and 12c show the evolution of a and b constants with Δy_p, respectively. A good fitting was found with polynomial models, as can be seen. It is important to notice that there is a huge sensitivity of PICC relatively to small errors of a and b constants, therefore these must be modelled quite accurately.

3.3.4. Application of the model

A finite element analysis is required to obtain Δy_p along crack flank. Fixing the position of crack tip, the distance of individual plastic wedges to crack tip can be calculated and used in equation 7 along with Δy_p to obtain the contribution of individual plastic wedges to PICC level. The global value of PICC produced by the residual plastic field is obtained summing the contributions of all individual plastic wedges behind crack tip, considering the linear superposition principle.

This model was applied to different situations, in order to test its accuracy and the validity of the premises behind it. Figure 13 shows the results obtained with the application of an overload with K_{OL}=7.3 MPa.m$^{1/2}$ after a crack extension of 0.369 mm (baseline loading: K_{min}=0, K_{max}=6.4 MPa.m$^{1/2}$). The results of Δy_p presented in figure 13a show a peak of plastic deformation corresponding to the application of the overload. The peak extends over a region,

ACCEPTED MANUSCRIPT

because the plastic deformation associated with the overload extends ahead of the crack tip. Figure 13b compares the PICC values obtained from the finite element method with those calculated using the empirical model based on equation 7. The excellent agreement between the curves validates the analytical model and the methodology followed to deduce it, namely the linear superposition principle, and the use of vertical plastic elongation to quantify the effect of residual plastic wake.

4. Discussion

The main objective of the present paper is to propose a parameter for the establishment of quantitative links between physical parameters, residual plastic field behind crack tip and PICC level. The vertical elongation of plastic wedges, Δy_p, obtained numerically from the integration of vertical plastic deformation perpendicularly to crack flank, was selected since it has an obvious physical meaning. This concept is similar to the difference in opening displacements between the stationary and the fatigue cracks, proposed by other authors [25-27, 29]. In fact, the analysis of crack profiles is an alternative to equation 5 that can be exploited.

The good correlation of this parameter with PICC level is a strong indication of its adequacy for PICC analysis. A second validation was searched using the empirical model proposed in previous section. The good agreement between numerical predictions and the empirical model validated the premises behind it, namely that the vertical plastic elongation is a key parameter for PICC analysis. The values observed for Δy_p were relatively small within micron range, indicating that a small plastic elongation is enough to produce PICC. Camas [47] found differences of about 5 μm between crack profiles obtained with and without crack propagation at the surface of CT specimens, therefore within the ranges obtained here. Singh *et al.* [28] obtained values of about 3 μm. Anyway, the increase of plastic deformation level, by mesh refinement or by the increase of the number of load cycles, is expected to increase the

ACCEPTED MANUSCRIPT

magnitude of Δy_p. The variation of PICC level with Δy_p, presented in figure 8, indicates a saturation of PICC for relatively high values of Δy_p, which is not completely understood.

The empirical model proposed in previous section does not include the effects of other phenomena, like crack tip blunting. This apparent disadvantage is effectively interesting since it permits the isolation of the effect of residual plastic wedges, from other phenomena. Figure 14 shows the results obtained with the application of load blocks, as illustrated. Three load blocks were considered, all with K_{min}=0 while K_{max}=4.6, 2.7 and 6.4 MPa.m$^{1/2}$. The decrease of K_{max} from 4.6 to 2.7 MPa.m$^{1/2}$ decreased the plastic deformation level, as is evident in figure 14a, but the decrease is not drastic which may be explained by the plastic deformation ahead of crack tip at the end of the first block. On the other hand, the subsequent load increase to 6.4 MPa.m$^{1/2}$ is immediately observed in Δy_p. The analytical model of PICC predicts variations respecting the changes of Δy_p. However, there is a significant difference between the FEM predictions and the empirical model in the intermediate region. Apparently, what is happening at the current crack tip has a significant influence on PICC level, not included in the present model. Sehitoglu *et al.* [48] observed that a crack blunting mechanism in plane strain competes with the closure mechanism. The phenomenon of partial closure [49] can also be used to explain the differences observed. The CJP model [45,50,51] also studies the shielding effect of the plastic enclave surrounding the crack. It considers the retarding effect of plastic strain at crack flanks and crack tip, and the compatibility-induced shear stress at the elastic-plastic interface. Two new stress intensity factors are defined, an interfacial shear stress intensity factor, K_S, and a retarding stress intensity factor, K_R. Also the crack tip stress field characterised by the stress intensity factor K_I and the T-stress are included, so the model has 4 parameters. The CJP model produces results that reflect blunting effects.

ACCEPTED MANUSCRIPT

Finally, most of the plastic deformation takes place close to the crack flank, therefore focus must be placed there. The size and orientation of crack tip plastic zone, which has been widely studied in literature, seems to have a limited effect on Δy_p and PICC level.

4. Conclusions

A single parameter was proposed here to quantify the magnitude of residual plastic deformation behind crack tip. The Δy_p parameter is the elongation of residual plastic wedges perpendicularly to crack flank and is obtained by the integration of vertical plastic deformation perpendicularly to crack flank. A well defined link was found between PICC level and Δy_p, indicating that this can be used to understand and quantify the effects of physical parameters on plasticity induced crack closure. Other main conclusions are:

- the plastic deformation at each Gauss Point (GP) accumulates progressively as the crack tip approaches it. It is a complex process involving monotonic and reversed plastic deformations, material hardening and strain ratcheting. When the crack tip moves ahead the GP plastic deformation ceases, and the existing deformation is part of the residual plastic field. The residual plastic deformation depends on the physical and numerical parameters, namely the position of the GP relatively to crack flank, the mesh refinement, the number of load cycles, the hardening material properties and the load parameters;

- crack closure happens mainly in a small region behind crack tip. More than 50 % of crack closure occurs within a distance of 0.1 mm behind crack tip. Therefore, experimental techniques used for direct observations of crack faces contact must look to the region immediately behind crack tip. Additionally, the first horizontal layer of elements, close to crack flank, has a significant influence on the global value of PICC (up to 50%), which increases with maximum load. The size of forward plastic zone apparently plays a minor role on PICC phenomenon;

ACCEPTED MANUSCRIPT

- the residual plastic wake may be seen as a set of vertical plastic wedges. The linear superposition principle applies to the effect of these individual plastic wedges on PICC level, which could be expected considering that the material behaves elastically behind crack tip;

- the influence of individual plastic wedges on PICC exponentially decreases with the distance to the crack tip, *d*. This conclusion was consistently observed using different approaches, namely with isolated plastic wedges, constant amplitude tests and overload situations. The effect an individual plastic wedge was found to disappear for distances to crack tip greater than one millimetre;

- an empirical model was developed assuming that Δy_p is the parameter controlling PICC, that the linear superposition principle is valid and that the influence of Δy_p decreases exponentially with distance to crack tip, *d*. The model relates PICC level of individual plastic wedges with distance to crack tip, *d*, and plastic deformation level, Δy_p. The global PICC is obtained summing the contributions of individual plastic wedges behind crack tip. A good agreement was found between the empirical model and FEM results, which was an additional validation of Δy_p concept.

Acknowledgments

The authors are indebted to the Portuguese Foundation for the Science and Technology (FCT) and COMPETE program from FEDER (European Regional Development Fund) for the financial support under the Projects PTDC/EME-PME/114892/2009 and PEst-C/EME/UI0285/2013.

References

[1] Ritchie RO, Suresh S, Moss CM. Near-threshold fatigue crack growth in 2(1/4)Cr-1 Mo pressure vessel steel in air and hydrogen. J of Engineering Materials and Technology 1980;**102**:293-299.

ACCEPTED MANUSCRIPT

[2] Suresh S, Ritchie RO. On the influence of fatigue underloads on cyclic crack growth at low stress intensities. Materials Science and Engineering 1981;**51**:61-69.

[3] Suresh S, Ritchie RO. A geometric model for fatigue crack closure induced by fracture surface morphology. Metallurgical Transactions 1982;**13A**:1627-1631.

[4] Elber W. The significance of fatigue crack closure under cyclic tension. In: *Damage tolerance in aircraft structures*, Philadelphia: ASTM STP 486, American Society for Testing and Materials; 1971, p.230-242.

[5] Blom AF, Holm DK. An experimental and numerical study of crack closure. Eng Fract Mech 1984; **22**:997-1011.

[6] Borrego LP, Ferreira JM, Costa JM. Fatigue crack growth and crack closure in an AlMgSi alloy. Fatigue Fract Eng Mater Struct 2001;**24**:255-265.

[7] KTV Rao, W, Yu, RO Ritchie, "On the behaviour of small fatigue cracks in comercial aluminum lithium alloys, Eng Fract Mech 1988, 31(4), 623-635.

[8] Bao H, McEvily AJ. On Plane Stress-Plane Strain Interactions in Fatigue Crack Growth. Int. J Fatigue 1998;**20**(6):441-448.

[9] Costa JDM, Ferreira JAM. Effect of Stress Ratio and Specimen Thickness on Fatigue Crack Growth of CK45 Steel. Theoretical and Applied Fracture Mechanics 1998;30:65-73.

[10] Yu HC, Tanaka K, Akiniwa Y. Estimation of torsional fatigue strength of medium carbon steel bars with circumferential crack by the cyclic resistance-curve method. Fatigue Fract Eng Mater 1998; 21: 1067-1076.

[11] Tanaka K. Crack initiation and propagation in torsional fatigue of circumferentially notched steel bars. Int J Fatigue 2013; in press, available online, http://dx.doi.org/10.1016/j.ijfatigue.2013.01.002.

[12] Berto F, Lazzarin P, Yates J. Multiaxial fatigue of V-notched steel specimens: a non-conventional application of the local energy method. Fatigue Fract Engng Mater Struct 2011; 34: 921-943.

[13] Elber W. Fatigue crack closure under cyclic tension. Eng. Fracture Mechanics 1970;**2**:37-45.

[14] Solanki K, Daniewicz SR, Newman JR. JC. Finite element analysis of plasticity-induced crack closure: an overview. Eng Fract Mech 2004;**71**:149-171.

ACCEPTED MANUSCRIPT

[15] Solanki K, Daniewicz SR, Newman JR. JC. Finite element modelling of plasticity-induced crack closure with emphasis on geometry and mesh refinement effects. Eng Fract Mech 2003;70: 1475-1489.

[16] González-Herrera A, Zapatero J. Influence of minimum element size to determine crack closure stress by the finite element method. Eng Fract Mech 2005;**72**:337-355.

[17] de Matos PFP, Nowell D., "on the accurate assessment of crack opening and closing stresses in plasticity-induced fatigue crack closure problems", Eng Fract Mech 2007;74:1579-1601,.

[18] Pommier S, Freitas M. Effect on fatigue crack growth of interactions between overloads. Fatigue Fract Eng Mater Struct 2002;**25**:709-722.

[19] Zapatero J, Moreno B, González-Herrera A. Fatigue crack closure determination by means of finite element analysis. Eng Fract Mech 2008;**75**:41-57.

[20] Rodrigues DM, Antunes FV. Finite element simulation of plasticity induced crack closure with different material constitutive models. Eng Fract Mech 2009;**76**:1215–1230.

[21] Cochran KB, Dodds RH, Hjelmstad KD. The role of strain ratcheting and mesh refinement in finite element analysis of plasticity induced crack closure", Int. J Fatigue 2011;**33**:1205-1220.

[22] McClung RC, Sehitoglu H., "On the finite element analysis of fatigue crack closure-1: Basic modelling issues. Eng Fract Mech 1989;33(2):237-252

[23] Wu J, Ellyin F. A study of fatigue crack closure by elastic-plastic finite element analysis for constant-amplitude loading. Int. J Fract 1996;82:43-65.

[24] Zhao LG, Tong J, Byrne J. The evolution of the stress-strain fields near a fatigue crack tip and plasticity-induced crack closure revisited. Fatigue Fract Eng Mater Struct 2004;**27**; 19-29.

[25] Newman Jr JC. A finite element analysis of fatigue crack closure. ASTM STP 1976;590:281–301.

[26] McClung RC, Sehitoglu, H. On the finite element analysis of fatigue crack closure-2: Numerical results. Eng Fract Mech 1989;33:253-272

[27] S. Roychowdhury, R. H. Dodds Jr., "Three-dimensional effects on fatigue crack closure in the small-scale yielding regime – a finite element study", Fatigue Fract Eng Mater Struct 26; 663-673:2003.

ACCEPTED MANUSCRIPT

[28] Singh KD, Khor KH, Sinclair I. Finite element and analytical modelling of crack closure due to repeated overloads. Acta Materialia 2008;**56**:835-851.

[29] Roychowdhury S, Dodds Jr. RH. Effect of T-stress on fatigue crack closure in 3-D small-scale yielding. Int J Solids Struct 2004;41:2581-2606.

[30] Vor K, Gardin C, Sarrazin-Baudoux C, Petit J. Wake Length and loading history effects on crack closure of through-thickness long and short cracks in 304L: PartII 3D numerical simulation. Eng Fract Mech 2013;**99**:306-323.

[31] de Matos PFP, Nowell D. Numerical simulation of plasticity-induced fatigue crack closure with emphasis on the crack growth scheme: 2D and 3D analysis, Eng Fract Mech 2008;**75**: 2087-2114.

[32] Hill R (1948) A theory of the yielding and plastic flow of anisotropic metals. Proceedings of Mathematical, Physical and Engineering Science, Royal Society London, 1948.

[33] Chaparro BM, Thuillier S, Menezes LF, Manach PY, Fernandes JV. Material parameters identification: Gradient-based, genetic and hybrid optimization algorithms. Computational Materials Science 2008;**44**(2):339-346.

[34] Menezes LF, Teodosiu C. Three-Dimensional Numerical Simulation of the Deep-Drawing Process using Solid Finite Elements. J of Materials Processing Technology 2000;**97**:100-106.

[35] Oliveira MC, Alves JL, Menezes LF. Improvement of a frictional contact algorithm for strongly curved contact problems. Int J for Numerical Methods in Eng 2003;**58**(14):2083-2101.

[36] Oliveira MC, Alves JL, Chaparro BM, Menezes LF. Study on the influence of work-hardening modeling in spring-back prediction. Int J of Plasticity 2007;**23**:516–543.

[37] Alves JL, Menezes LF. Application of tri-linear and tri-quadratic 3-D solid FE in sheet metal forming process simulation. In: K. Mori, editors. NUMIFORM 2001, Japan, 2001;639–644.

[38] Oliveira MC, Menezes LF. Automatic correction of the time step in implicit simulations of the stamping process. Finite Elements in Analysis and Design 2004;**40**:1995–2010.

[39] Antunes FV, Rodrigues DM. Numerical simulation of plasticity induced crack closure: Identification and discussion of parameters. Eng Fract Mech 2008;**75**:3101–3120.

ACCEPTED MANUSCRIPT

[40] Suresh S, Ritchie RO. A geometric model for fatigue crack closure induced by fracture surface roughness. Metallurgical Transactions 1982:**13A**:1627-1631.

[41] J Wásen, B Karlson. The relation between fracture surface geometry and crack closure in fatigue. Proc. Fourth Int. Conference on Fatigue and Fatigue Thresholds (Fatigue 90), Eds H Kitagawa and T Tanaka.

[42] Iyyer NS, Dowling NE. Opening and Closing of cracks at high cyclic strains. 2nd Eng Foundation Int Conference and Workshop on Small Fatigue Cracks, 213-223, Metall. Soc. AIME, Warrendale PA., 1986.

[43] Paris PC, Tada H, Donald JK. Service load fatigue damage – a historical perspective. Int J Fatigue 1999;21:S35-S46.

[44] Zerbst U, Madia M, Hellmann D. An analytical fracture mechanics model for estimation of S–N curves of metallic alloys containing large second phase particles. Eng Fract Mech 2012;82:115–134.

[45] Christopher CJ, James MN, Patterson EA, Tee KF. Towards a new model of crack tip stress fields. Int J of Fracture 2007; 148 (4):361-371.

[46] Solancki K, Daniewicz SR, Newman Jr. JC. A new methodology for computing crack opening values from finite element analyses. Eng Fract Mech 2004; **71**: 1165-1175.

[47] Camas D. Numerical study of the Three-Dimensional Behaviour of Plasticity Induced Crack Closure Phenomenon in Bi-dimensional specimens. PhD Thesis, University of Málaga; 2013.

[48] Sehitoglu H, Sun W. Modelling of plane strain fatigue crack closure. J Eng Mater Tech, 1991;**113**:31- 40.

[49] Borrego LP, Ferreira JM, Costa JD. Partial crack closure under block loading. Int J Fatigue 2008; **30**:1787-1796.

[50] Christopher CJ, James MN, Patterson EA, Tee KF. A quantitative evaluation of fatigue crack shielding forces using photoelasticity. Eng Fract Mech 2008;75:4190–4199.

[51] James MN, Christopher CJ, Lu Y, Patterson EA. Local crack plasticity and its influences on the global elastic stress field. Int J of Fatigue 2013;46:4-15.

ACCEPTED MANUSCRIPT

ACCEPTED MANUSCRIPT

ACCEPTED MANUSCRIPT

List of figures

List of tables

ACCEPTED MANUSCRIPT

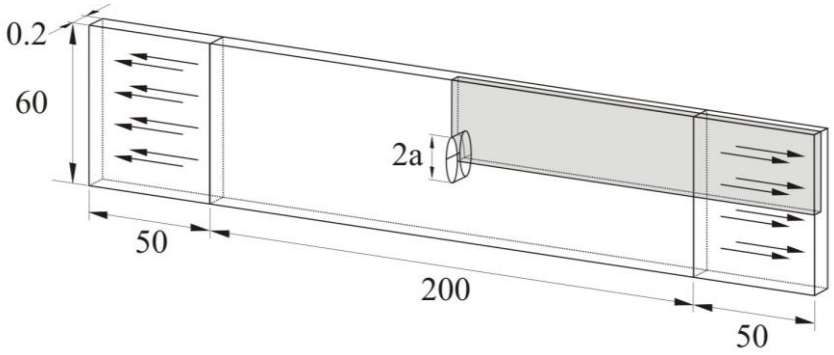

Figure 1

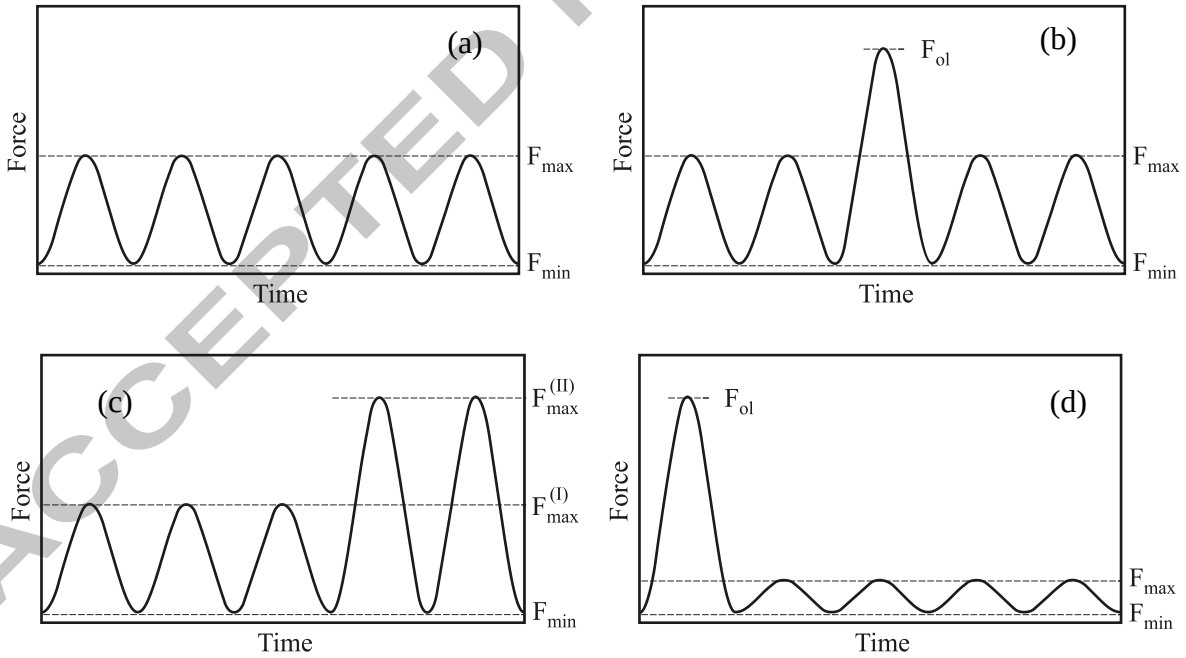

Figure 2

ACCEPTED MANUSCRIPT

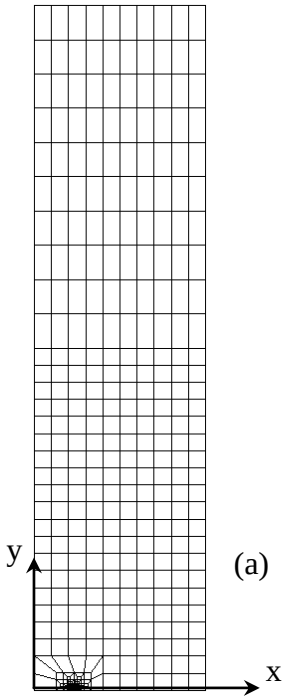

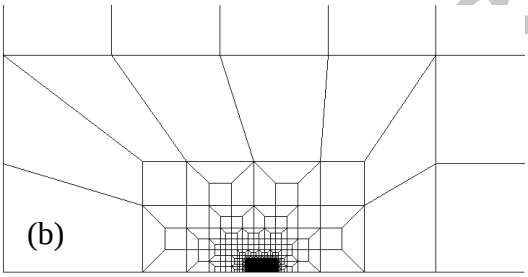

Figure 3

ACCEPTED MANUSCRIPT

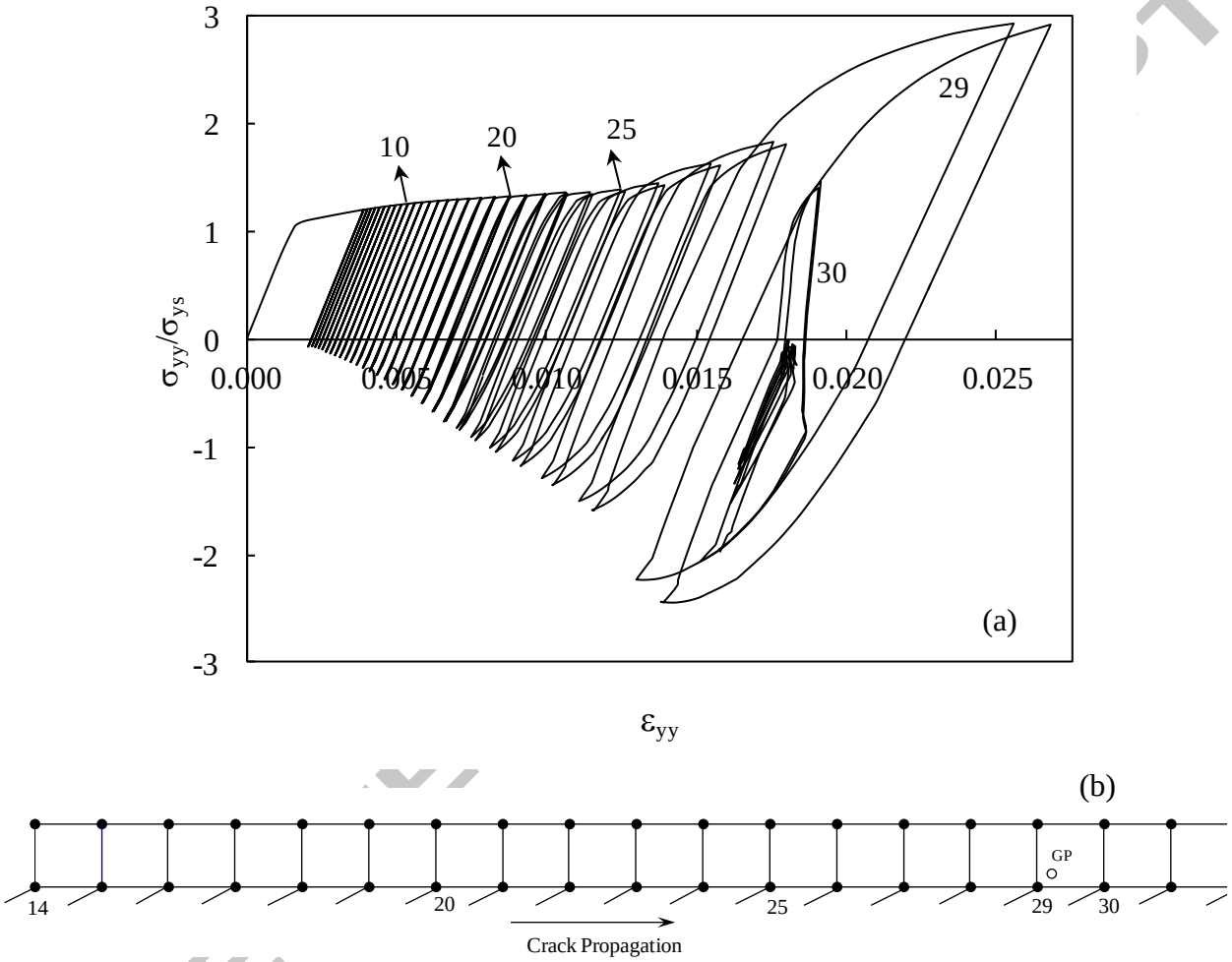

Figure 4

ACCEPTED MANUSCRIPT

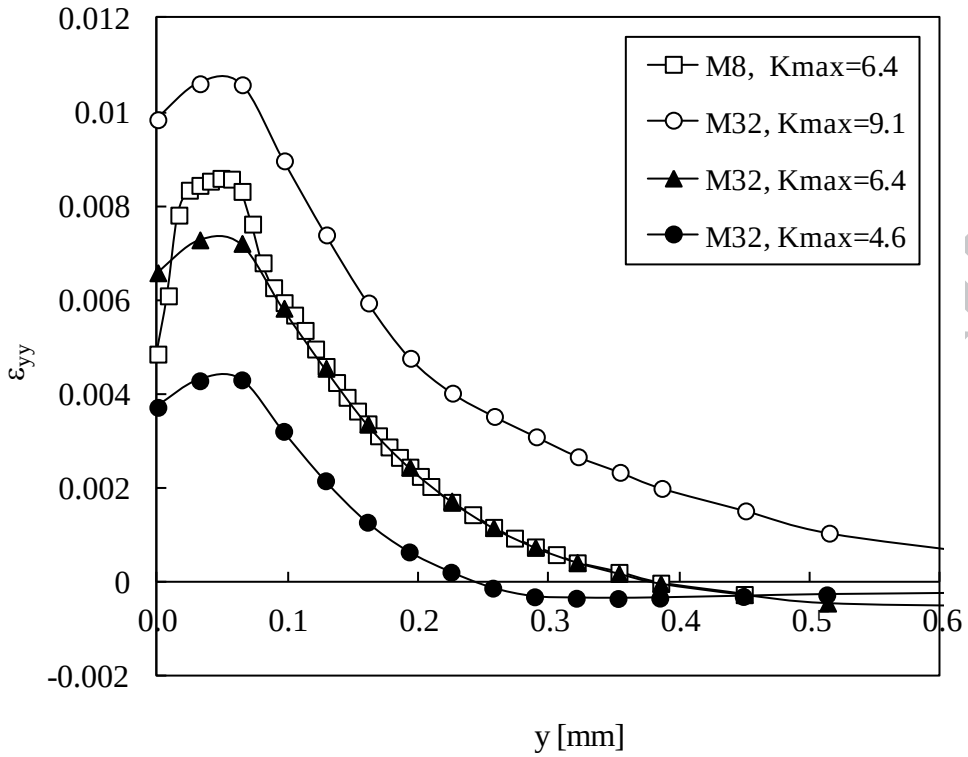

Figure 5

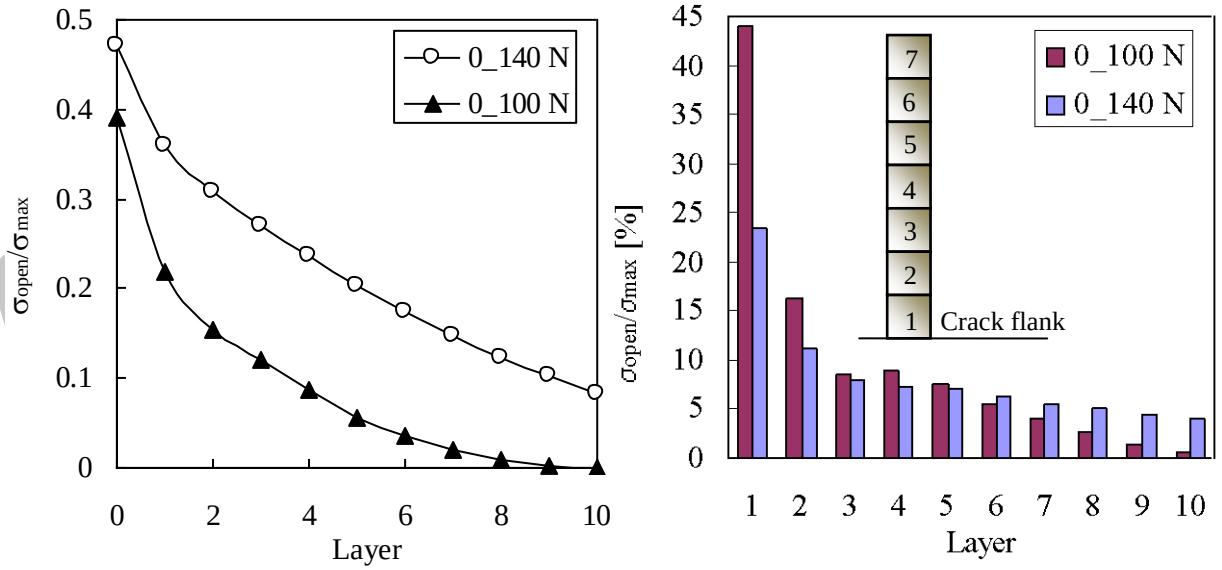

Figure 6

ACCEPTED MANUSCRIPT

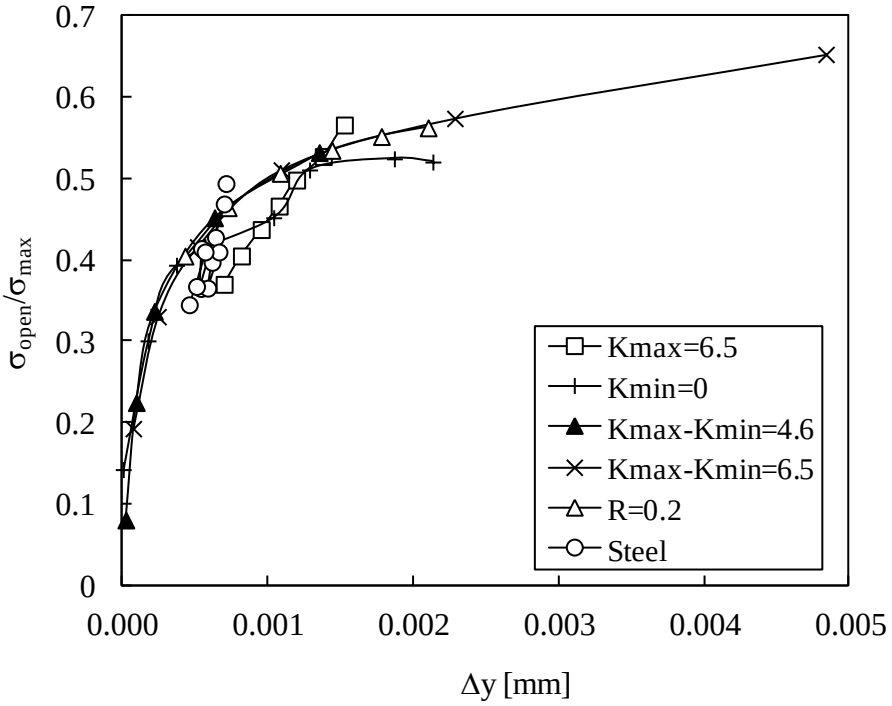

Figure 7

ACCEPTED MANUSCRIPT

ACCEPTED MANUSCRIPT

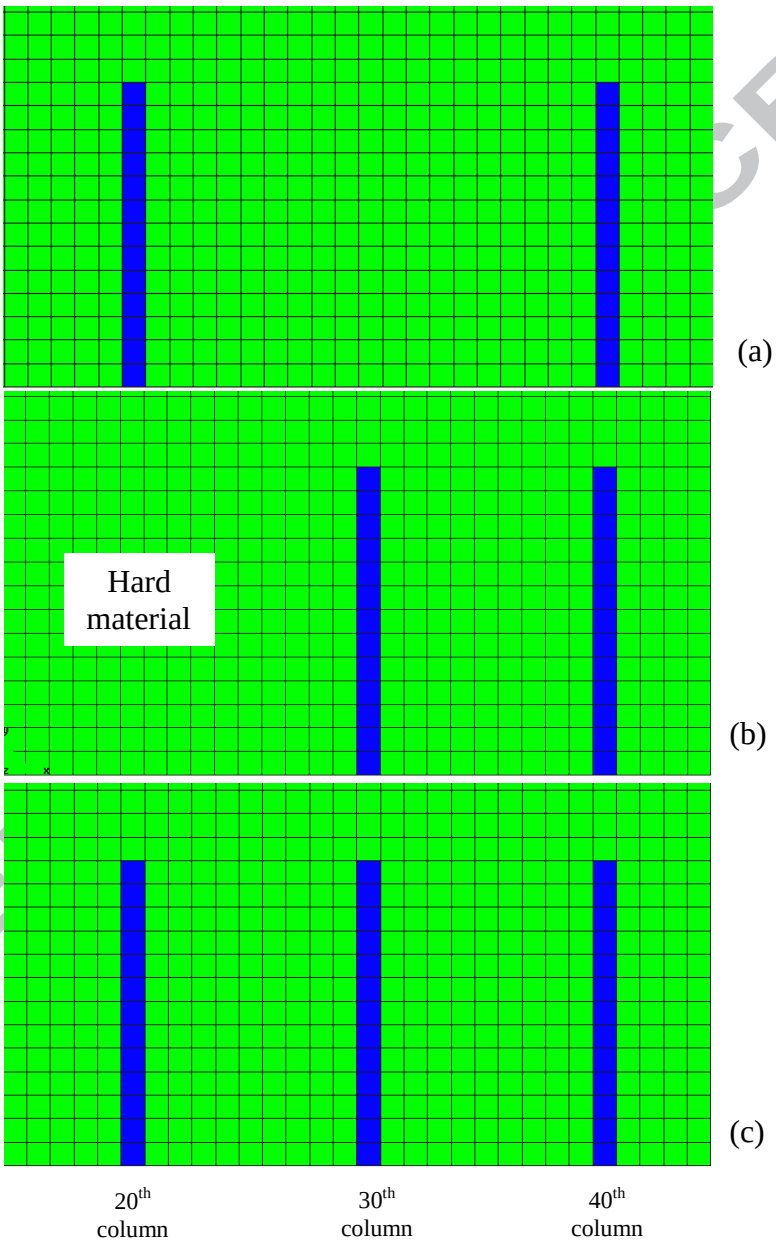

Figure 8

ACCEPTED MANUSCRIPT

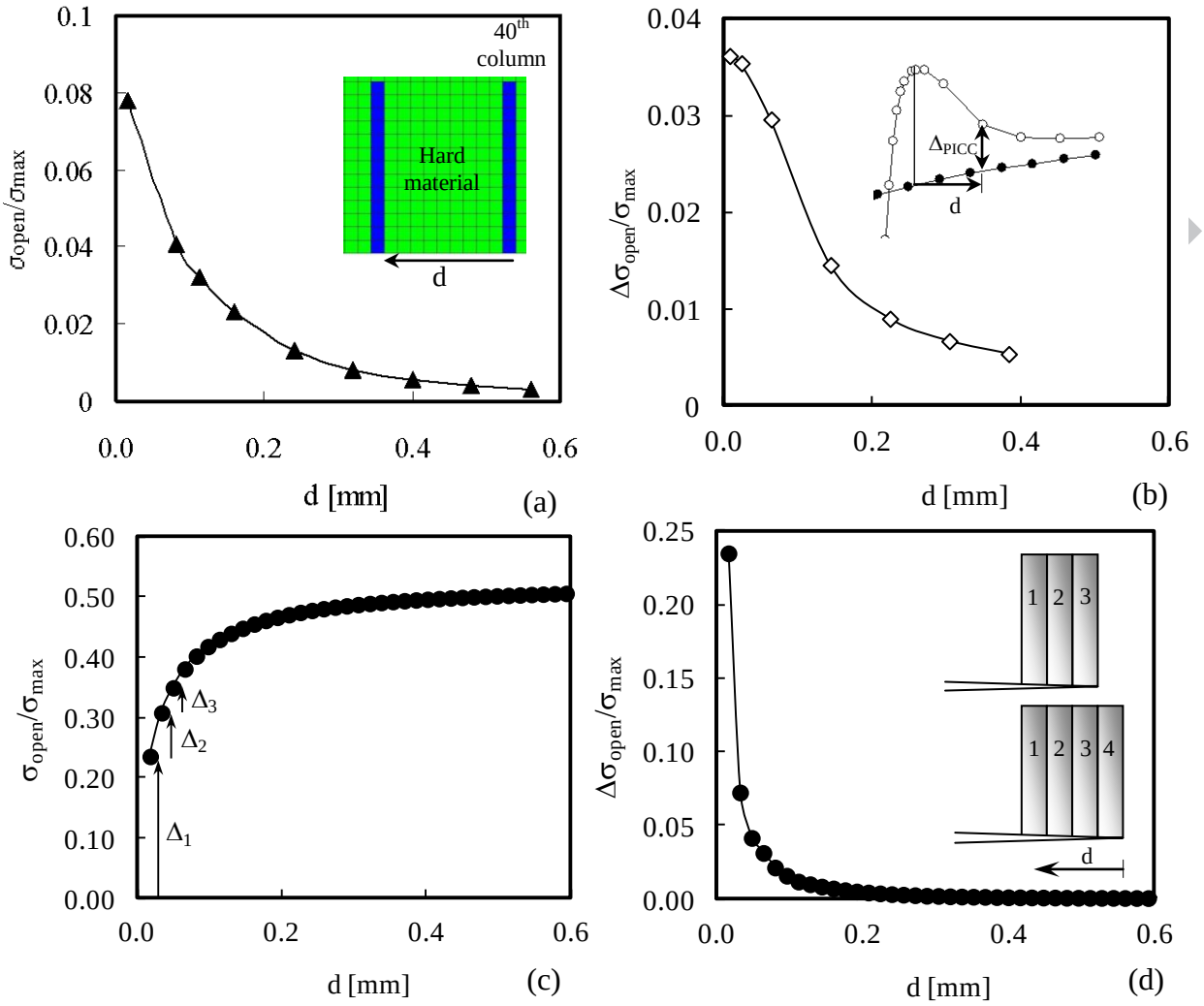

Figure 9

ACCEPT

ACCEPTED MANUSCRIPT

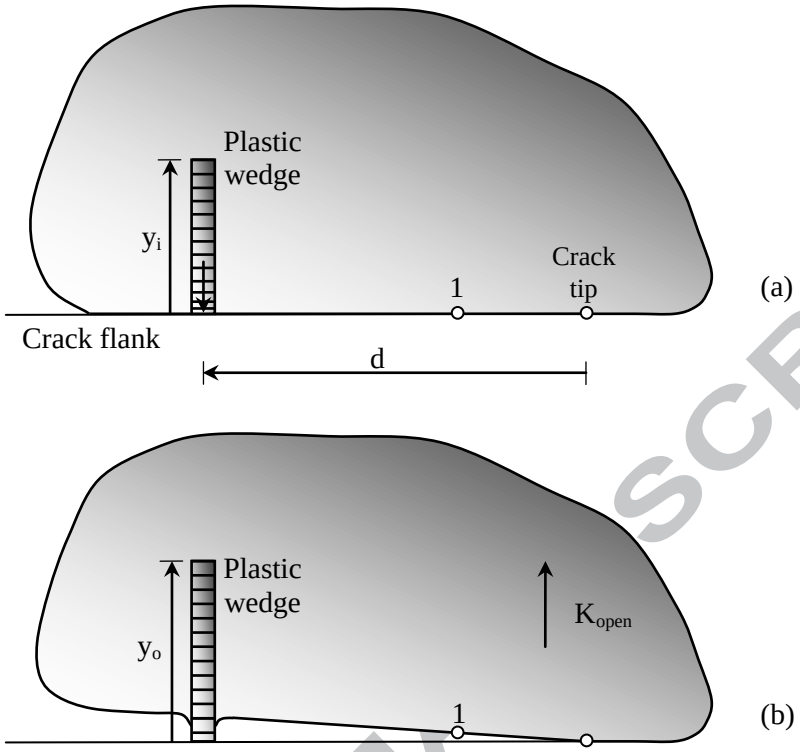

Figure 10

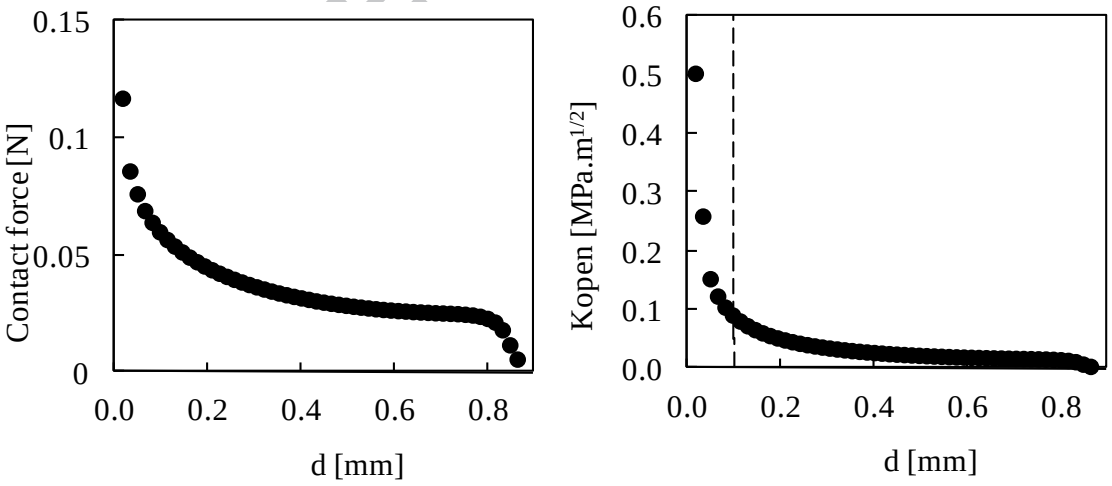

Figure 11

ACCEPTED MANUSCRIPT

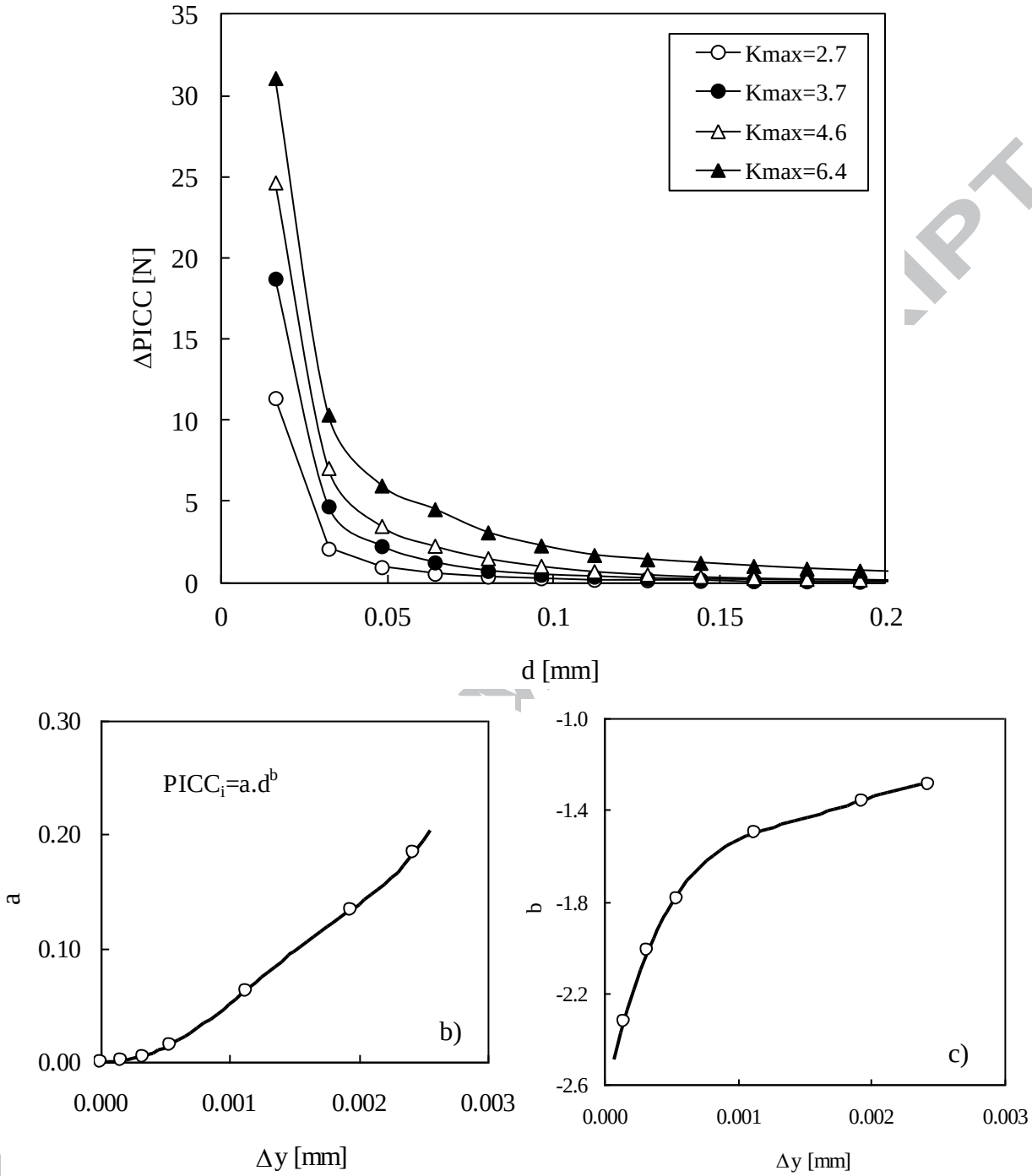

Figure 12

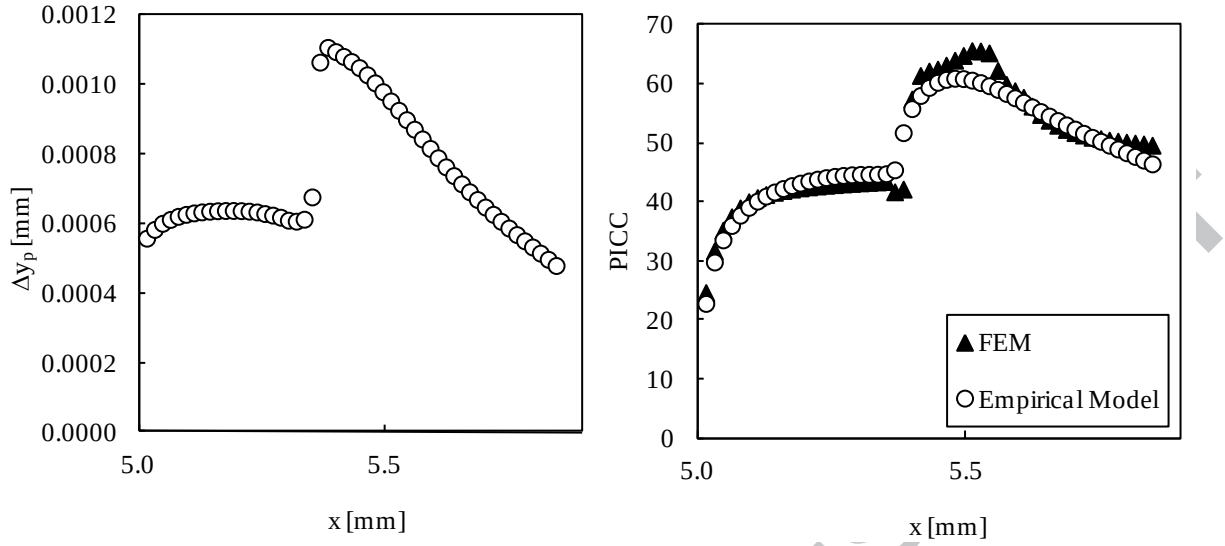

Figure 13

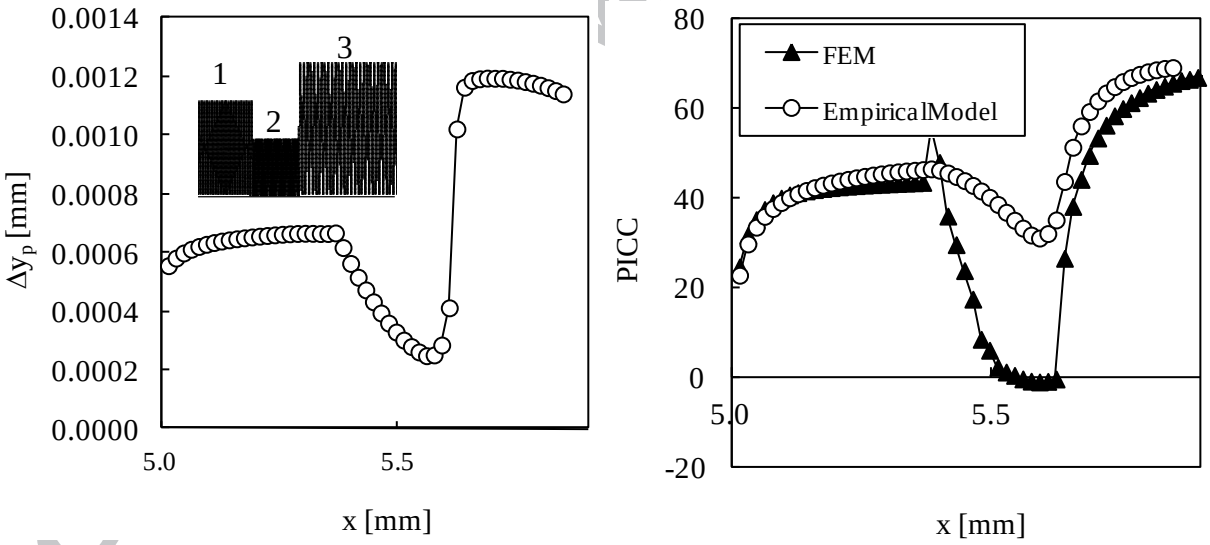

Figure 14

ACCEPTED MANUSCRIPT

Table 1. Load level in constant amplitude tests.

Loadcase	F_{min} [N]	F_{max} [N]	σ_{max} [MPa]	σ_{max}/σ_{ys}
1	0	60	20	0.16
2	0	80	26.7	0.22
3	0	100	33.3	0.27
4	0	140	46.7	0.38
5	0	180	60	0.48
6	0	200	66.7	0.54
7	0	220	73.3	0.59

ACCEPTED MANUSCRIPT